Inorganic Chemistry

ARTICLE

pubs.acs.org/IC

Family of Double-Cubane Mn_4Ln_2 (Ln = Gd, Tb, Dy, Ho) and Mn_4Y_2 Complexes: A New Mn_4Tb_2 Single-Molecule Magnet

Arpita Saha,[†] Michael Thompson,[†] Khalil A. Abboud,[†] Wolfgang Wernsdorfer,[‡] and George Christou*[,†]

[†]Department of Chemistry, University of Florida, Gainesville, Florida 32611-7200, United States

[‡]Institut Néel, CNRS, BP 166, 25 Avenue des Martyrs, 38042 Grenoble, Cedex 9, France

Supporting Information

ABSTRACT: The synthesis and characterization of a family of $Mn_2^{III}Mn_2^{II}Ln^{III}_2$ complexes (Ln = Gd (**1**), Tb (**2**), Dy (**3**), and Ho (**4**)) of formula $[Mn_4Ln_2O_2(O_2CBu^t)_6(edteH_2)_2(NO_3)_2]$ are reported, where $edteH_4$ is *N,N,N′,N′*-tetrakis(2-hydroxyethyl)ethylenediamine. The analogous Mn_4Y_2 (**5**) complex has also been prepared. They were obtained from reaction of $Ln(NO_3)_3$ or $Y(NO_3)_3$ with $Mn(O_2CBu^t)_2$, $edteH_4$, and NEt_3 in a 2:3:1:2 molar ratio. The crystal structures of representative **1** and **2** were obtained, and their core consists of a face-fused double-cubane $[Mn_4Ln_2(\mu_4\text{-}O^{2-})_2(\mu_3\text{-}OR)_4]$ unit. Such double-cubane units are extremely rare in 3d metal chemistry and unprecedented in 3d−4f chemistry. Variable-temperature, solid-state dc and ac magnetic susceptibility studies on **1**−**5** were carried out. Fitting of dc χ_MT vs T data for **5** gave J_{bb} ($Mn^{III}\cdots Mn^{III}$) = −32.6(9) cm^{-1}, J_{wb} ($Mn^{II}\cdots Mn^{III}$) = +0.5(2) cm^{-1}, and g = 1.96(1), indicating a $|n, 0, n\rangle$ (n = 0−5) 6-fold-degenerate ground state. The data for **1** indicate an S = 12 ground state, confirmed by fitting of magnetization data, which gave S = 12, D = 0.00(1) cm^{-1}, and g = 1.93(1) (D is the axial zero-field splitting parameter). This ground state identifies the $Mn^{II}\cdots Gd^{III}$ interactions to be ferromagnetic. The ac susceptibility data independently confirmed the conclusions about **1** and **5** and revealed that **2** displays slow relaxation of the magnetization vector for the Mn_4Tb_2 analogue **2**. The latter was confirmed as a single-molecule magnet by observation of hysteresis below 0.9 K in magnetization vs dc field scans on a single crystal of **2**·MeCN on a micro-SQUID apparatus. The hysteresis loops also displayed well-resolved quantum tunneling of magnetization steps, only the second 3d−4f SMM to do so.

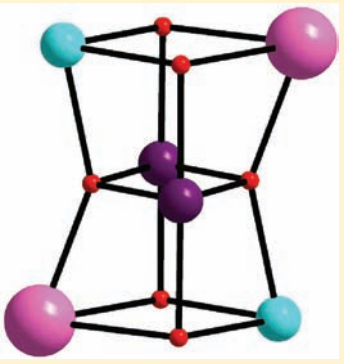

INTRODUCTION

Polynuclear 3d transition metal cluster chemistry continues to attract workers from around the world owing to the fascinating structural architectures such molecules often possess and the fascinating properties they often exhibit. Our own interest, and that of many other groups, has centered on manganese chemistry, a metal whose Mn/O cluster chemistry is of relevance to many diverse areas, from bioinorganic chemistry areas such as the oxygen-evolving complex of photosynthesis,[1] through molecules with abnormally high-spin (S) values,[2] or molecular refrigerant properties,[3] to single-molecule magnets (SMMs).[4−6] SMMs are molecules with a significant barrier to magnetization relaxation as a result of a combination of a high ground state spin (S) value and easy axis magnetic anisotropy. SMMs also straddle the classical/quantum interface by displaying not just classical magnetization hysteresis but also quantum tunneling of magnetization (QTM)[7] and quantum phase interference.[8] These properties make SMMs potential candidates for use as quantum bits (qubits) in quantum computation.[9] More recently, mixed 3d−4f clusters have attracted much interest in the SMM field as workers have sought to amalgamate the often large spin and anisotropy of Ln^{3+} (Ln = lanthanide) ions, particularly Tb^{3+}, Dy^{3+}, and Ho^{3+}, with the propensity of Mn_x clusters to possess large spin S values. As a result, the first 3d−4f SMM, a Cu_2Tb_2 complex, was reported in 2004[10] and also later that year the first Mn−Ln SMM, a Mn_6Dy_6 complex.[11] In the subsequent several years, a large number of other Mn−Ln clusters have been reported,[3,12] spanning various nuclearities such as Mn_2Ln_2, Mn_2Ln_3, Mn_4Ln_4, Mn_4Ln_3, Mn_4Ln_6, Mn_5Ln_4, Mn_6Ln_2, Mn_6Dy_6, Mn_9Dy_8, $Mn_{10}Ln_2$, $Mn_{11}Dy_4$, $Mn_{11}Gd_2$, $Mn_{12}Gd$, $Mn_{18}Dy$, and $Mn_{21}Dy$. Preparation of these clusters has involved the use of polydentate chelating ligands, *N*-substituted di- and triethanolamines, carboxylate groups, and tripodal ligands. All these ligands feature either alcohol or carboxylate arms which, upon deprotonation, foster formation of high-nuclearity products.

More recently, our group has been exploring the potentially *N,N,O,O,O,O*-hexadentate chelate *N,N,N′,N′*-tetrakis(2-hydroxyethyl)ethylenediamine ($edteH_4$) in transition metal chemistry. To date, both Mn and Fe homometallic clusters of various nuclearities have been obtained, establishing this chelate as a flexible ligand in transition metal chemistry as a result of its four alcohol/alkoxide arms,[13] and therefore, we more recently turned our attention to employing it in mixed 3d−4f cluster chemistry. In the present work, we describe the initial exploration of $edteH_4$ in Mn−Ln chemistry in the presence of carboxylate groups as

Received: August 3, 2011
Published: September 22, 2011

coligands. We report the syntheses, crystal structures, and magnetic characterization of a family Mn_4Ln_2 (Ln = Gd, Tb, Dy, Ho) complexes with an unprecedented 3d−4f metal topology consisting of a face-fused double cubane. We also report the corresponding Mn_4Y_2 complex containing diamagnetic Y^{III} atoms to assist the magnetic studies. In addition, the Tb analogue has been found to be a new addition to the SMM family.

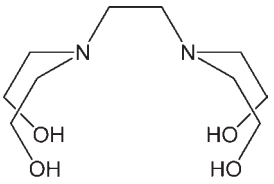

edteH$_4$

EXPERIMENTAL SECTION

Syntheses. All preparations were performed under aerobic conditions using reagents and solvents as received. $Mn(O_2CBu^t)_2$ was synthesized as described in the literature.[14]

[$Mn_4Gd_2O_2(O_2CBu^t)_6(edteH_2)_2(NO_3)_2$] (**1**). To a stirred solution of edteH$_4$ (0.20 g, 0.84 mmol) and NEt_3 (0.25 mL, 1.68 mmol) in MeCN/MeOH (20/1, v/v) was added $Mn(O_2CBu^t)_2$ (0.66 g, 2.52 mmol). The resulting red-brown solution was stirred for 20 min under mild heating, and then $Gd(NO_3)_3$ (0.76 g, 1.68 mmol) was added to the solution and stirred for a further 2 h. The solution was then filtered and the filtrate left undisturbed at room temperature. X-ray-quality, orange-brown plate-like crystals of **1**·3MeCN slowly grew over 2 days, and they were collected by filtration, washed with Et_2O, and dried under vacuum; the yield was 12%. Anal. Calcd (Found) for **1** (solvent free): C, 34.01 (33.73); H, 5.59 (5.56); N, 4.76 (4.67). Selected IR data (cm^{-1}): 3405 (br), 2967 (m), 2678 (w), 1566 (s), 1484 (s), 1415 (br, s), 1308 (m), 1228 (s), 1072 (s), 1032 (m), 897 (m), 795 (w), 741(w), 594 (br, s), 530 (w), 454 (m).

[$Mn_4Tb_2O_2(O_2CBu^t)_6(edteH_2)_2(NO_3)_2$] (**2**). Preparation is similar to that for **1**, except that $Tb(NO_3)_3$ (0.73 mg, 1.68 mmol) was used as the Ln salt. The crystals were identified crystallographically as **2**·MeCN, but vacuum-dried solid analyzed as solvent free. The yield was 15%. Anal. Calcd (Found) for **2** (solvent free): C, 33.95 (33.78); H, 5.58 (5.58); N, 4.75 (4.71). Selected IR data (cm^{-1}): 3393 (br), 2967 (m), 2906 (m), 2679 (w), 1566 (s), 1484 (s), 1416 (br, s), 1309 (m), 1228 (s), 1114 (w), 1072 (s), 1031 (m), 925 (w), 898 (m), 795 (m), 743 (w), 594 (br, s), 531 (w), 454 (m).

[$Mn_4Dy_2O_2(O_2CBu^t)_6(edteH_2)_2(NO_3)_2$] (**3**). Preparation is similar to that for **1**, except that $Dy(NO_3)_3$ (0.58 mg, 1.68 mmol) was used as the Ln salt. The yield was 15%. Anal. Calcd (Found) for **3** (solvent free): C, 33.81 (33.61); H, 5.56 (5.58); N, 4.73 (4.98). Selected IR data (cm^{-1}): 3392 (br), 2970 (w), 2739 (w), 2677 (w), 1567 (s), 1484 (s), 1412 (br, s), 1311 (m), 1228 (s), 1171 (w), 1072 (s), 1033 (s), 926 (w), 898 (s), 825 (m), 794 (w), 744 (w), 595 (br, s), 533 (w), 455 (m).

[$Mn_4Ho_2O_2(O_2CBu^t)_6(edteH_2)_2(NO_3)_2$] (**4**). Preparation is similar to that for **1**, except that $Ho(NO_3)_3$ (0.74 mg, 1.68 mmol) was used as the Ln salt. The yield was 15%. Anal. Calcd (Found) for **4** (solvent free): C, 33.72 (33.54); H, 5.55 (5.54); N, 4.72 (4.73). Selected IR data (cm^{-1}): 3370 (br), 2967 (br), 2678 (w), 1567 (s), 1418 (br, s), 1312 (s), 1227 (s), 1114 (w), 1072 (s), 1031 (s), 897 (s), 820 (w), 795 (w), 746 (w), 595 (br, s), 533 (w), 455 (m).

[$Mn_4Y_2O_2(O_2CBu^t)_6(edteH_2)_2(NO_3)_2$] (**5**). Preparation is similar to that for **1**, except that $Y(NO_3)_3$ (0.58 mg, 1.68 mmol) was used. The yield was 14%. Anal. Calcd (Found) for **5** (solvent free): C, 36.87 (36.58); H, 6.06 (6.01); N, 5.16 (5.18). Selected IR data (cm^{-1}): 3396 (br), 2967 (s), 2905 (m), 1567 (s), 1484 (s), 1417 (s), 1374 (m), 1314 (m), 1228 (s), 1072 (vs), 1032 (s), 925 (m), 898 (m), 818 (w), 796 (w), 747 (w), 594 (br, s), 530 (w), 456 (m).

Table 1. Crystallographic Data for 1·3MeCN and 2·MeCN

parameter	1	2
formula	$C_{56}H_{103}Gd_2Mn_4N_9O_{28}$	$C_{52}H_{97}Mn_4N_7O_{28}Tb_2$
fw, g/mol	1884.73	1805.97
cryst syst	monoclinic	monoclinic
space group	*C*2/*c*	*C*2/*c*
a, Å	24.733(4)	24.2909(15)
b, Å	13.810(2)	14.4236(9)
c, Å	22.262(4)	21.8221(13)
β, deg	104.651(9)	109.987(1)
V, Å^3	7357(2)	7185.1(8)
Z	4	4
T, K	100(2)	100(2)
radiation, Å[a]	0.71073	0.71073
ρ, g/cm^3	1.702	1.669
μ, mm^{-1}	2.527	2.705
R1[b,c]	0.0368	0.0300
wR2[d]	0.0901	0.0606

[a] Graphite monochromator. [b] $I > 2\sigma(I)$. [c] $R1 = \Sigma(||F_o| - |F_c||)/\Sigma|F_o|$. [d] $wR2 = [\Sigma w(F_o^2 - F_c^2)^2]/\Sigma[w(F_o^2)^2]^{1/2}$, $w = 1/[\sigma^2(F_o^2) + [(ap)^2 + bp]$, where $p = [F_o^2 + 2F_c^2]/3$.

X-ray Crystallography. Data were collected for **1**·3MeCN and **2**·MeCN at 100 K on a Bruker DUO system equipped with an APEX II area detector and a graphite monochromator utilizing Mo Kα radiation (λ = 0.71073 Å). Cell parameters were refined using 9999 reflections. A hemisphere of data was collected using the ω-scan method (0.5° frame width). Absorption corrections by integration were applied based on measured indexed crystal faces. The structure was solved by direct methods in SHELXTL6 and refined on F^2 using full-matrix least-squares cycles. The non-H atoms were treated anisotropically, whereas the H atoms were placed in calculated, ideal positions and refined as riding on their respective C atoms. Unit cell data and structure refinement details are listed in Table 1.

For **1**·3MeCN, the asymmetric unit consists of a half Mn_4Gd_2 cluster on an inversion center and 1.5 solvent MeCN molecules (the half molecule is located on a 2-fold rotation axis). Fragment O2−C9−C10 was disordered and refined in two parts. A total of 448 parameters were refined in the final cycle of refinement using 5716 reflections with $I > 2\sigma(I)$ to yield R_1 and wR_2 of 3.68 and 9.01%, respectively.

For **2**·MeCN, the asymmetric unit consists of half a Mn_4Tb_2 cluster on an inversion center and half a MeCN solvent molecule. The latter was too disordered to be modeled properly; thus, the program SQUEEZE,[15] a part of the PLATON package of crystallographic software, was used to calculate the solvent disorder area and remove its contribution to the overall intensity data. There are two disordered regions in the cluster. The C10−O4 group of the edteH$_4$ ligand is disordered and refined in two parts with their site occupation factors dependently refined. The three methyl groups on atom C22 are disordered and were treated in the same manner. In the final cycle of refinement, 8260 reflections (of which 6090 are observed with $I > 2\sigma(I)$) were used to refine 403 parameters and the resulting R1 and wR_2 of 3.00 and 6.06%, respectively.

Physical Measurements. Infrared spectra were recorded in the solid state (KBr pellets) on a Nicolet Nexus 670 FTIR spectrometer in the 400−4000 cm^{-1} range. Elemental analyses (C, H, and N) were performed by the in-house facilities of the University of Florida,

dx.doi.org/10.1021/ic201683p |*Inorg. Chem.* 2011, 50, 10476–10485

Chemistry Department. Variable-temperature dc and ac magnetic susceptibility data were collected at the University of Florida using a Quantum Design MPMS-XL SQUID susceptometer equipped with a 7 T magnet and operating in the 1.8−300 K range. Samples were embedded in solid eicosane to prevent torquing. Magnetization vs field and temperature data were fit using the program MAGNET.[16] Pascal's constants were used to estimate the diamagnetic correction, which was subtracted from the experimental susceptibility to give the molar paramagnetic susceptibility (χ_M). Low-temperature (<1.8 K) magnetic measurements were performed in Grenoble using an array of micro-SQUIDs.[17] The field can be applied in any direction by separately driving three orthogonal coils. The applied field was aligned parallel to the easy axis (z axis) of the molecules using a published method.[18] The high sensitivity of this magnetometer allows the study of single crystals of the order of 10−500 μm.

RESULTS AND DISCUSSION

Syntheses. A variety of reaction systems involving different reagent ratios and solvent media was explored to develop the procedure described here. Reaction of edteH$_4$ with Mn(O$_2$CBu^t)$_2$, Gd(NO$_3$)$_3$, and NEt$_3$ in a 1:3:2:2 molar ratio in MeCN/MeOH (10/1, v/v) afforded a red-brown solution from which [Mn$_4$Gd$_2$O$_2$(O$_2$CBu^t)$_6$(edteH$_2$)$_2$(NO$_3$)$_2$] (**1**; Mn$^{III}_2$Mn$^{II}_2$Gd$^{III}_2$) was subsequently isolated in 12% yield. Its formation is summarized in eq 1

$$4Mn(O_2CR)_2 + 2Gd(NO_3)_3 + 2edteH_4 + 4NEt_3 + H_2O + 0.5O_2 \rightarrow [Mn_4Gd_2O_2(O_2CR)_6(edteH_2)_2(NO_3)_2] + 2Bu^tCO_2H + 4NHEt_3NO_3 \quad (1)$$

The NEt$_3$ functions as a proton acceptor, as well as providing the basic conditions to facilitate oxidation of Mn^{II} to Mn^{III} by atmospheric O$_2$ gas. Using only MeCN as the solvent also leads to the same product, but the mixed-solvent system led to the most crystalline product in the highest yield. The same product in comparable yield was obtained using Mn(NO$_3$)$_2$, MnCl$_2$, or Mn(ClO$_4$)$_2$ and ^{t}BuCO$_2$H in a 1:2 molar ratio instead of Mn(O$_2$CBu^t)$_2$. The reaction scheme was general and successfully yielded the analogous Mn$_4$Ln$_2$ compounds with Ln = Tb (**2**), Dy (**3**), and Ho (**4**) as well the corresponding Mn$_4$Y$_2$ (**5**) complex. In all cases the yields were low (12−15%), but the products were reproducibly obtained in highly crystalline and analytically pure forms, the latter no doubt assisted by them crystallizing directly from a reaction solution that probably contains a mixture of products. Indeed, the filtrates were still highly colored, but we were not able to isolate additional crops of Mn$_4$Ln$_2$ complexes from them.

Description of Structures. The partially labeled structure, a stereoview, and the core of **1** are presented in Figure 1; selected interatomic distances and angles are listed in Table 2. The centrosymmetric molecule possesses a [Mn$_4$Gd$_2$O$_2$(OR)$_4$]$^{8+}$ core (Figure 1, bottom) consisting of a face-fused, double cubane comprising four Mn and two Gd atoms bridged by two μ_4-O^{2-} (O5) and four μ_3-OR$^-$ (O1, O4) groups. The two edteH$_2^{2-}$ groups are each hexadentate chelating on a Mn^{II} atom (Mn1), and their two deprotonated alkoxide arms provide the μ_3-OR$^-$ groups bridging the Mn^{II} atom to the neighboring Mn^{III} (Mn2) and Gd atoms. The edteH$_2^{2-}$ groups are thus in an overall η^1:η^1:η^1:η^1:η^3:η^3:μ_4 ligation mode, as shown in Figure 2. The

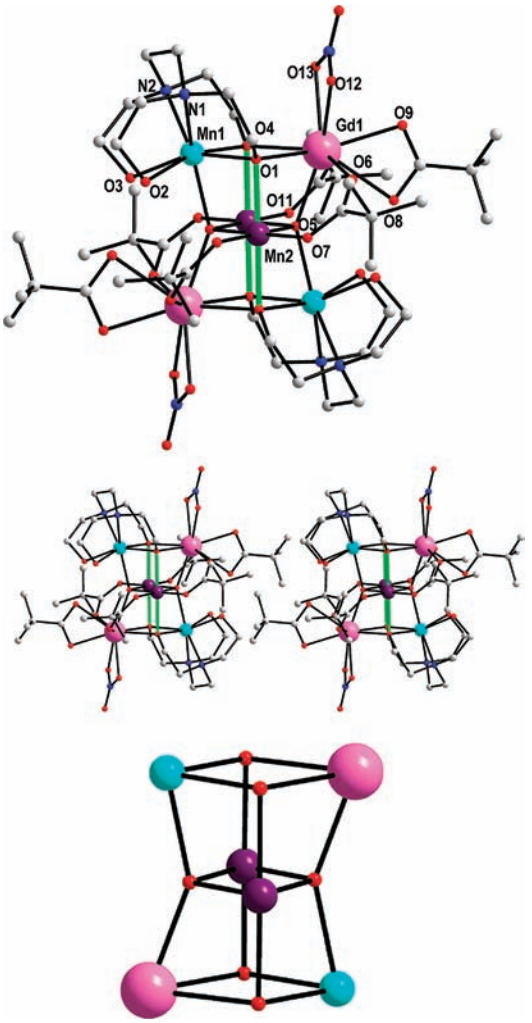

Figure 1. Partially labeled structure (top), stereopair (middle), and face-fused double-cubane core (bottom) of centrosymmetric **1**. Mn^{III} JT axes are shown as green lines. Hydrogen atoms have been omitted for clarity. Color code: Mn^{III}, purple; Mn^{II}, cyan; Gd, pink; O, red; N, blue; C, light gray.

four Mn^{III}Gd pairs are each additionally bridged by a carboxylate group in their common syn,syn η^1:η^1:μ mode, and the peripheral ligation is completed by a chelating ^{t}BuCO$_2^-$ and a chelating NO$_3^-$ on each Gd. As a result, Mn1 (Mn^{II}), Mn2 (Mn^{III}), and the Gd are seven, six, and nine coordinate, respectively. The Mn oxidation states were confirmed by bond-valence sum (BVS) calculations (Table 3).[22]

The two Mn^{III} atoms are near-octahedral and display JT axial elongations along the O1−Mn2−O4 axes (green bonds in Figure 1, top). The elongated Mn−O bonds are >0.2 Å longer than the others, and the two JT axes are essentially parallel. The protonation level of all O atoms was determined by O (BVS) calculations (Table 4).[19] In particular, edteH$_2^{2-}$ O atoms O1 and O4 have BVS values of ∼2.0, confirming them to be deprotonated, as expected from their μ_3-bridging modes. In contrast, O2 and O3 have values of 1.45 and 1.29, respectively, confirming them as protonated; the increased values from the expected 1.0−1.2 range are due to their involvement as donors in O−H···O hydrogen bonding, thereby lowering their apparent 'protonation level'. The significantly larger value for O2 is due

dx.doi.org/10.1021/ic201683p |Inorg. Chem. 2011, 50, 10476–10485

Table 2. Selected Interatomic Distances (Å) and Angles (deg)[a] for 1·3MeCN

Mn(2)···Mn(2′)	2.8813(14)	Mn(1)···Mn(2′)	3.1442(9)
Mn(2)···Mn(1′)	3.1442(9)	Mn(1)···Mn(2)	3.1673(11)
Mn(2)···Gd(1′)	3.3195(8)	Gd(1)···Mn(2′)	3.3195(8)
Gd(1)−O(5)	2.331(3)	Mn(1)−O(5′)	2.275(3)
Gd(1)−O(6)	2.364(3)	Mn(1)−O(2)	2.296(9)
Gd(1)−O(10)	2.415(3)	Mn(1)−N(2)	2.335(5)
Gd(1)−O(4)	2.442(3)	Mn(1)−O(3)	2.344(4)
Gd(1)−O(9)	2.445(4)	Mn(1)−N(1)	2.379(3)
Gd(1)−O(1)	2.470(3)	Mn(2)−O(5′)	1.902(3)
Gd(1)−O(12)	2.495(3)	Mn(2)−O(5)	1.916(3)
Gd(1)−O(13)	2.498(4)	Mn(2)−O(11′)	1.954(4)
Gd(1)−O(8)	2.586(3)	Mn(2)−O(7)	1.964(4)
Mn(1)−O(4)	2.176(3)	Mn(2)−O(1)	2.163(3)
Mn(1)−O(1)	2.192(3)	Mn(2)−O(4′)	2.221(3)
Mn(2)−O(1)−Gd(1)	92.26(10)	Mn(2′)−O(5)−Mn(1′)	98.24(12)
Mn(1)−O(1)−Gd(1)	107.89(12)	Mn(2)−O(5)−Mn(1′)	96.88(15)
Mn(1)−O(4)−Mn(2′)	91.30(14)	Mn(2′)−O(5)−Gd(1)	102.83(15)
Mn(1)−O(4)−Gd(1)	109.42(13)	Mn(2)−O(5)−Gd(1)	103.61(11)
Mn(2′)−O(4)−Gd(1)	90.65(11)	Mn(1′)−O(5)−Gd(1)	148.03(16)
Mn(2′)−O(5)−Mn(2)	98.01(16)	Mn(2)−O(1)−Mn(1)	93.31(12)

[a] Primed and unprimed atoms are related by symmetry.

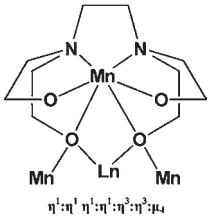

Figure 2. Coordination mode of the edteH$_2^{2-}$ groups in **1** and **2**.

to its forming two such contacts in a bifurcated hydrogen bond (O2···O8 = 2.846 Å and O2···O11 = 2.850 Å), whereas O3 forms a single contact (O3···O8 = 2.677 Å).

The partially labeled structure of complex **2** is presented in Figure 3; selected interatomic distances and angles are listed in Table 5. The structure of **2** is almost superimposable with that of **1**, except that the Ln atom is not Tb^{III}. In particular, the Mn oxidation states were confirmed by BVS calculations (Table 3), and the Mn^{III} JT axes are again parallel. As expected, there are only small differences in interatomic distances and angles. As a result and because elemental analyses and IR spectra indicated the other products were also all isostructural with **1** and **2**, the crystal structures of **3**, **4**, and **5** were not pursued.

The face-fused, {M$_6$O$_6$} double-cubane topology is a very rare structural type. There is no previous example of such a discrete unit in 3d−4f chemistry, but four homometallic Mn$_6$ examples have been reported: [Mn$_6$O$_4$(OMe)$_2$(O$_2$CMe)$_4$(Mesalim)$_4$] (Mesalim$^-$ = methyl salicylimidate anion),[20a] [Mn$_6$O$_4$(OMe)$_2$(O$_2$CPh)$_4$(dphmp)$_4$] (dphmp$^-$ = the anion of diphenyl(pyridine-2-yl)methanol),[20b] [Mn$_6$O$_4$(OMe)$_2$(O$_2$CMe)$_4$(Hpzbg)$_4$] (Hpzbg$^-$ = monopyrazolyl biguanide anion),[20c] and [Mn$_6$O$_2$(teaH$_2$)$_4$(O$_2$CMe)$_4$] (teaH$_2^-$ = the monoanion of triethanolamine).[20d] Apart from the Mn$_6$ vs Mn$_4$Ln$_2$ difference, the cores of these complexes differ from those of **1** and **2** in other ways: (i) the homometallic complexes are Mn$^{III}_6$[20a−c] or Mn$^{II}_4$Mn^{III}Mn^{IV},[20d] whereas **1** and **2** are Mn$^{II}_2$Mn$^{III}_2$Ln$^{III}_2$, and (ii) the Mn$_6$ cores contain four O^{2-} and two MeO$^-$ ions, except one[20d] that has two O^{2-} and four RO$^-$ as in **1** and **2**. A heterometallic complex containing a {M$_6$O$_6$} double-cubane subunit is also known.[21]

Table 3. Bond-Valence Sums[b] for the Mn Atoms of 1 and 2[a]

complex	atom	Mn^{2+}	Mn^{3+}	Mn^{4+}
1	Mn1	2.24	2.09	2.04
	Mn2	3.39	3.13	3.07
2	Mn1	3.35	3.09	3.04
	Mn2	2.23	2.13	2.07

[a] The oxidation state of a particular atom is the nearest integer to the underlined value. [b] The underlined value is the closest to the charge for which it was calculated.

Magnetochemistry: Direct Current Magnetic Susceptibility Studies. Solid-state, variable-temperature dc magnetic susceptibility (χ_M) measurements were performed on vacuum-dried microcrystalline samples of complexes **1**−**5**. The data were collected in the 5.0−300 K range in a 0.1 T (1000 Oe) dc magnetic field, and they are shown as $\chi_M T$ vs T plots in Figure 4. For **1**−**4**, the $\chi_M T$ at 300 K are in the 27.71−39.52 cm^3 K mol^{-1} range, a little smaller than the expected values for a noninteracting Mn$_4$Ln$_2$ system, as summarized in Table 6. Upon lowering the temperature, $\chi_M T$ stays fairly constant down to the 20−50 K region and then increases markedly to 48.76−70.39 cm^3 K mol^{-1} at 5.0 K (Table 6). The $\chi_M T$ at 5.0 K of 63.93 cm^3 K mol^{-1} for **1**, which contains two isotropic Gd^{III} atoms, suggests a ground state spin of S = 11 or 12 (spin-only g = 2.0 values are 66.0 and 78.0 cm^3 K mol^{-1}, respectively). For **5**, whose paramagnetism is only from the Mn atoms, the $\chi_M T$ decreases slightly from 11.36 cm^3 K mol^{-1} at 300 K to 8.02 cm^3 K mol^{-1} at 5.0 K.

The data for complex **5** were fit in order to determine the exchange interactions between Mn$_2$ pairs (Figure 5). If the Y atoms are ignored, the four Mn form an oxo-bridged Mn$_4$

dx.doi.org/10.1021/ic201683p |Inorg. Chem. 2011, 50, 10476–10485

Table 4. Bond-Valence Sums for the O Atoms of Complex 1[a]

atom	BVS	assignment	group
O1	2.05	RO^-	$edteH_2^{2-}$
O2	1.45	ROH	$edteH_2^{2-}$
O3	1.29	ROH	$edteH_2^{2-}$
O4	1.99	RO^-	$edteH_2^{2-}$
O5	1.96	O^{2-}	O^{2-}

[a] BVS values for O atoms of O^{2-}, ROH, and H_2O groups are typically 1.8−2.0, 1.0−1.2, and 0.2−0.4, respectively, but can be affected by hydrogen bonding.

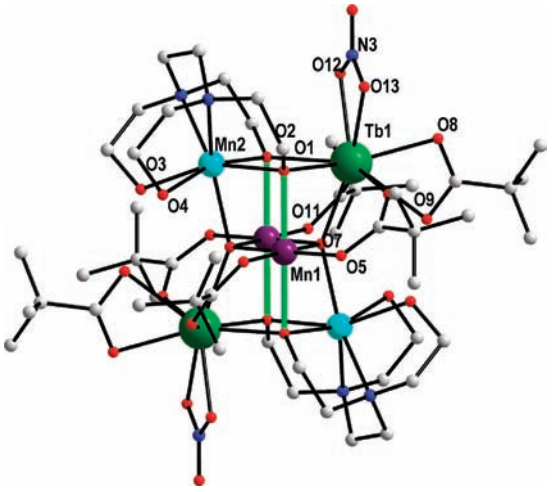

Figure 3. Partially labeled structure of complex **2**. Mn^{III} JT axes are shown as green lines. Hydrogen atoms have been omitted for clarity. Color code: Mn^{III}, purple; Mn^{II}, cyan; Tb, green; O, red; N, blue; C, light gray.

rhombus commonly called a 'defective dicubane'. The corresponding Heisenberg spin Hamiltonian is given by eq 2 using the atom labeling of Figure 5(inset (Mn1 = Mn3 = Mn^{III} and Mn2 = Mn4 = Mn^{II}))

$$\mathscr{H} = -2J_{wb}(\hat{S}_1\cdot\hat{S}_2 + \hat{S}_1\cdot\hat{S}_4 + \hat{S}_2\cdot\hat{S}_3 + \hat{S}_3\cdot\hat{S}_4) - 2J_{bb}\hat{S}_1\cdot\hat{S}_3 \quad (2)$$

$$E|S_T, S_A, S_B\rangle = -J_{wb}[S_T(S_T+1) - S_A(S_A+1) - S_B(S_B+1)] - J_{bb}[S_A(S_A+1)] \quad (3)$$

where J_{wb} and J_{bb} are $Mn^{II}Mn^{III}$ and $Mn^{III}Mn^{III}$ interactions, respectively. The eigenvalues of eq 2 are given by eq 3, where $\hat{S}_A = \hat{S}_1 + \hat{S}_3$, $\hat{S}_B = \hat{S}_2 + \hat{S}_4$, $\hat{S}_T = \hat{S}_A + \hat{S}_B$, S_T is the total spin of the molecule, and $E|S_T, S_A, S_B\rangle$ is the energy of state S_T arising from particular S_A and S_B.[22,23] There are 110 S_T states ranging in value from 0 to 9. These together with eq 3 and the Van Vleck equation were used to derive a theoretical $\chi_M T$ vs T expression for **5**, which was used to least-squares fit the experimental data in the 8.0−300 K range. Data below 8 K were ignored because the small decrease in $\chi_M T$ will likely be due to weak intermolecular interactions, ZFS, and/or Zeeman effects. The fit (solid line in Figure 5) gave $J_{bb} = -32.6(9)$ cm^{-1}, $J_{wb} = +0.5(2)$ cm^{-1}, and $g = 1.96(1)$, with temperature-independent paramagnetism (TIP) fixed at 400 × 10^{-6} cm^3 mol^{-1}. The obtained J_{bb} and J_{wb} values indicate a degenerate ground state for **5**, as evident in the S_T state energy diagram (Figure S1 of the Supporting Information). The ground state is 6-fold degenerate comprising the $|S_T, S_A, S_B\rangle = |0, 0, 0\rangle$, $|1, 0, 1\rangle$, $|2, 0, 2\rangle$, $|3, 0, 3\rangle$, $|4, 0, 4\rangle$, $|5, 0, 5\rangle$ states. This can be rationalized as follows: the large negative (antiferromagnetic, AF) value for J_{bb} leads to a ground state in which the Mn^{III} spins are aligned perfectly antiparallel, i.e., $S_A = 0$, and since it is assumed that there is no interaction between the distant Mn^{II} atoms (Mn2 and Mn4 in Figure 5, inset), the $S_B = 5, 4, 3, 2, 1,$ and 0 combinations of the two Mn^{II} spins are degenerate. The expected $\chi_M T$ for only this degenerate ground state being populated is 8.75 cm^3 K mol^{-1} for $g = 2.0$ and 8.40 ± 0.9 cm^3 K mol^{-1} for $g = 1.96(1)$ from the fit, close to the experimental value at 5.0 K. Of course, the ground state is unlikely to be truly 6-fold degenerate, since the long-distance $Mn^{II}Mn^{II}$ interactions are unlikely to be exactly zero. Nevertheless, the 5.0 K value suggests describing **5** as having a degenerate ground state is a reasonable approximation.

$J_{bb} < 0$ and $J_{wb} > 0$ represent competing exchange interactions (spin frustration) within the Mn_4 triangular subunits. However, $|J_{bb}| \gg J_{wb}$ for **5**, and thus the ferromagnetic (F) J_{wb} is overcome, leading to the degenerate ground state. The sensitivity of the spin state energies and resulting ground state to the J_{wb}/J_{bb} ratio is shown as E/J_{bb} vs J_{wb}/J_{bb} in Figure 6. For $|J_{wb}/J_{bb}| > 0.8$, the four F J_{wb} overcome the one AF J_{bb} and the spins all align parallel to give a $|9, 4, 5\rangle$ ground state. However, when $|J_{wb}/J_{bb}| < 0.2$, as found for **5**, the ground state is the degenerate $|n, 0, n\rangle$ ($n = 0-5$) state. At intermediate $0.8 < |J_{wb}/J_{bb}| < 0.2$ values, the ground state can be $|8, 3, 5\rangle$, $|7, 2, 5\rangle$, or $|6, 1, 5\rangle$, corresponding to the intermediate spin alignments defined by the S_A values. Similar situations of apparently degenerate ground states have been reported for $[Mn_4O_2]^{8+}$ complexes with a butterfly topology.[24]

It should be noted that in discrete homometallic $Mn^{III}_2Mn^{II}_2$ complexes with the defective-dicubane structure, both J_{bb} and J_{wb} are almost always F with $J_{bb} > J_{wb}$ and the complexes thus have an $S_T = 9$ ground state for all J_{wb}/J_{bb} ratios.[25] The obvious question is why does **5** have such a strong AF interaction? We believe the answer is to be found in the orientation of the Mn^{III} JT axes. The Mn_4 defective dicubanes almost always have μ_3-OR^- (R = H, alkyl) groups bridging each Mn_3 triangular subunit, and the JT axes align to include these and are thus 'in-plane' with respect to the central $Mn^{III}O_2Mn^{III}$ plane (case I in Figure 7). Since the JT axis defines the z axis of the singly occupied d_{z^2} orbital, this gives strong $d_{z^2}/d_{x^2-y^2}$ σ overlap with the empty $d_{x^2-y^2}$, which will be a major F contribution to the overall observed J_{bb}. In contrast, **5** has μ_3-O^{2-} ions and the JT axes avoid these, as JT axes usually do, and they are now oriented 'out of plane' (case II in Figure 7). The $d_{z^2}/d_{x^2-y^2}$ F overlap is lost, and the coupling is dominated by AF contributions giving an overall AF J_{bb}. Support for this explanation is provided by $[Mn_2Gd_2O_2(O_2CBu^t)_8(HO_2CBu^t)_2(MeOH)_2]$,[26] which has a defective-dicubane core with Mn^{III} atoms in the central positions (as in **5**) and two μ_3-O^{2-} bridges. The JT axes are out of plane, and the $Mn^{III}\cdots Mn^{III}$ coupling is $J_{bb} = -31.45$ cm^{-1}, very similar to that in **5**.

With the magnetism of **5** established, the $\chi_M T$ vs T plots for **1**−**4** in Figure 4 clearly indicate ferromagnetic Mn−Ln interactions to be present. For complex **1**, which contains two isotropic Gd^{III} ($S = 7/2$) atoms, the ground state was investigated with magnetization (M) data collected at 1.8−10 K in fields (H) up to 7 T. Data are plotted in Figure 8 as reduced magnetization ($M/N\mu_B$) vs H/T, where N is Avogadro's number and μ_B is the Bohr magneton. The saturation value is ~24.0, as expected for an

dx.doi.org/10.1021/ic201683p |Inorg. Chem. 2011, 50, 10476–10485

Table 5. Selected Interatomic Distances (Å) and Angles (deg)[a] for 2·MeCN

Mn(1)···Mn(1′)	2.8964(10)	Mn(1)···Mn(2′)	3.1609(7)
Mn(2)···Mn(1′)	3.1609(7)	Mn(1)···Mn(2)	3.1767(7)
Mn(1)···Tb(1′)	3.3210(5)	Tb(1)···Mn(1′)	3.1609(7)
Tb(1)−O(7)	2.318(2)	Mn(1)−O(2′)	2.213(2)
Tb(1)−O(6)	2.325(2)	Mn(1)−Mn(1′)	2.8964(10)
Tb(1)−O(10)	2.367(2)	Mn(1)−Mn(2′)	3.1609(7)
Tb(1)−O(8)	2.437(2)	Mn(1)−Mn(2)	3.1767(7)
Tb(1)−O(2)	2.459(2)	Mn(1)−Tb(1′)	3.3210(5)
Tb(1)−O(1)	2.460(2)	Mn(2)−O(2)	2.168(2)
Tb(1)−O(12)	2.475(2)	Mn(2)−O(4′)	2.198(6)
Tb(1)−O(13)	2.475(2)	Mn(2)−O(1)	2.203(2)
Tb(1)−O(9)	2.616(2)	Mn(2)−O(7′)	2.291(2)
Mn(1)−O(7′)	1.897(2)	Mn(2)−O(4)	2.330(6)
Mn(1)−O(7)	1.918(2)	Mn(2)−O(3)	2.342(3)
Mn(1)−O(5)	1.967(2)	Mn(2)−N(1)	2.343(3)
Mn(1)−O(11′)	1.973(2)	Mn(2)−N(2)	2.389(3)
Mn(1)−O(1)	2.176(2)		
Mn(1)−O(1)−Mn(2)	93.01(8)	Mn(1′)−O(7)−Mn(1)	98.8(1)
Mn(1)−O(1)−Tb(1)	92.04(8)	Mn(1′)−O(7)−Mn(2′)	98.21(9)
Mn(2)−O(1)−Tb(1)	108.61(9)	Mn(1)−O(7)−Mn(2′)	96.95(9)
Mn(2)−O(2)−Mn(1′)	92.37(8)	Mn(1′)−O(7)−Tb(1)	103.54(9)
Mn(2)−O(2)−Tb(1)	109.85(9)	Mn(1)−O(7)−Tb(1)	103.82(9)
Mn(1′)−O(2)−Tb(1)	90.46(7)	Mn(2′)−O(7)−Tb(1)	146.99(10)

[a] Primed and unprimed atoms are related by symmetry.

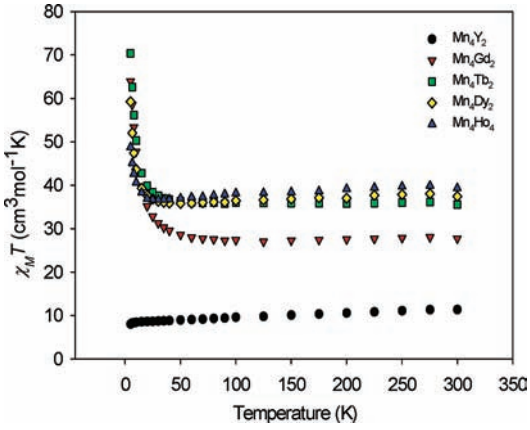

Figure 4. $\chi_M T$ vs T plots for complexes **1**−**5** in a 0.1 T (1000 Oe) dc field.

$S = 12$ spin state and $g \approx 2$. The data were fit using the program MAGNET,[16] which diagonalizes the spin Hamiltonian matrix assuming that only the ground state is populated, incorporating axial anisotropy ($D\hat{S}_z^2$) and Zeeman terms, and employing a full powder average. The corresponding spin Hamiltonian is given by eq 4, where $\hat{S}_z$ is the z-axis spin operator and μ_0 is the vacuum permeability

$$\mathscr{H} = D\hat{S}_z^2 + g\mu_B\mu_0\hat{S}\cdot H \quad (4)$$

The fit (solid lines in Figure 8) gave $S = 12$, $D = 0.00(1)$ cm^{-1}, and $g = 1.93(1)$. An equally good fit with $S = 11$, $D = 0.00(1)$ cm^{-1}, and $g = 2.10(1)$ was discarded due to the high g value. The very small D value was somewhat surprising given the orientation of the JT axes but is consistent with the essentially superimposed isofield lines (vide infra); the fit error surface (Figure S2 of the Supporting Information) shows no other fit minimum with a nonzero D. One remaining worry was that **1** might not really have an $S = 12$ ground state but instead the dc field was stabilizing an $S = 12$ excited state and making it seem that it was the ground state. To probe this possibility and to explore if **1**−**5** might exhibit slow magnetization relaxation, we turned to ac susceptibility studies.

Table 6. Summary of Direct Current Magnetic Data for Complexes 1−5[a]

compounds	Ln^{III}/Y^{III} free-ion ground state	$\chi_M T$ for noninteracting ions	exptl $\chi_M T$ at 300 K	exptl $\chi_M T$ at 5 K
Mn_4Gd_2 (**1**)	$^8S_{7/2}$	30.51	27.71	63.93
Mn_4Tb_2 (**2**)	$^7F_6$	38.39	35.57	70.39
Mn_4Dy_2 (**3**)	$^6H_{15/2}$	43.09	37.42	59.24
Mn_4Ho_2 (**4**)	$^5I_8$	42.89	39.52	48.76
Mn_4Y_2 (**5**)	$^1S_0$	14.75	11.36	8.02

[a] Units: cm^3 K mol^{-1}.

Alternating Current Magnetic Susceptibility Studies. These were performed on microcrystalline samples of **1**−**5** in a 3.5 Oe ac field oscillating at 5−1500 Hz. The in-phase (χ'_M) ac susceptibility is invaluable for assessing S without any complications from a dc field, and this is plotted in Figure 9 as $\chi'_M T$ vs T in the 1.8−15 K range at 250 Hz. For **5**, $\chi'_M T$ is essentially constant down to ∼4 K at ∼8.6 cm^3 K mol^{-1}, consistent with a well-isolated and degenerate $|n, 0, n\rangle$ ($n = 0$−5) state. There is a slight decrease below 4 K, but this is very slight and consistent with

dx.doi.org/10.1021/ic201683p |Inorg. Chem. 2011, 50, 10476–10485

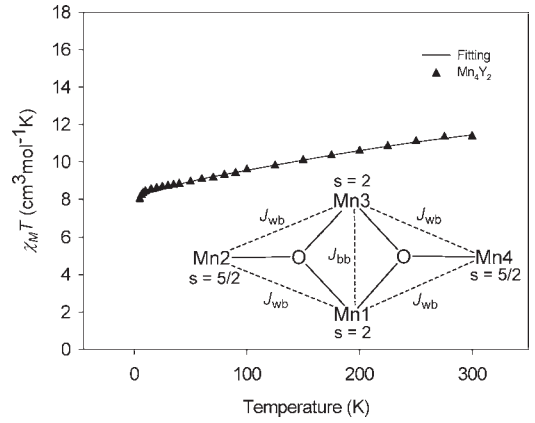

Figure 5. Fit of the $\chi_M T$ vs T data for **5** using the $2 - J$ coupling model shown as the inset. Solid line is the fit of the data; see text for fit parameters.

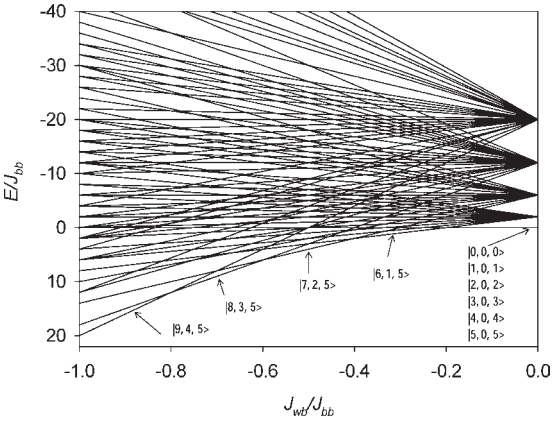

Figure 6. Energies, normalized to J_{bb}, of the spin states of **5** as a function of the J_{wb}/J_{bb} ratio for the $J_{wb} > 0$ and $J_{bb} < 0$ situation.

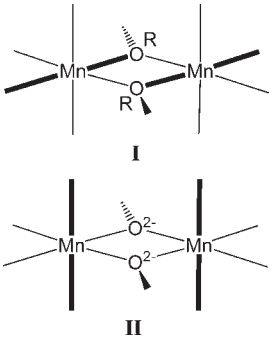

Figure 7. (I) Central $Mn^{III}_2(\mu_3\text{-}OR^-)_2$ unit of a Mn_4 defective dicubane with $J_{bb} > 0$ showing the in-plane orientation of the JT elongation axes (thick bonds). (II) Central $Mn^{III}_2(\mu_3\text{-}O^{2-})_2$ unit of **5** with $J_{bb} < 0$ showing the out-of-plane orientation of the JT axes.

essentially no ZFS or significant long-distance interaction between the Mn^{II} atoms. The ac data thus confirm the conclusions from the dc studies. For **1**, $\chi'_M T$ increases with decreasing T, indicating depopulation of excited states with a smaller S than the ground state, and reaches a plateau value of ~76 cm^3 K mol^{-1} consistent with $S = 12$ and $g \approx 1.97$, again confirming the

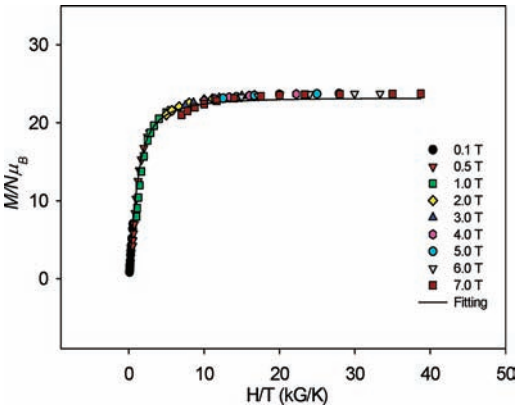

Figure 8. Reduced magnetization $(M/N\mu_B)$ vs H/T plots for **1** at applied fields of 0.1−7.0 T in the 1.8−10 K temperature range. Solid lines are the fit of the data; see text for fit parameters.

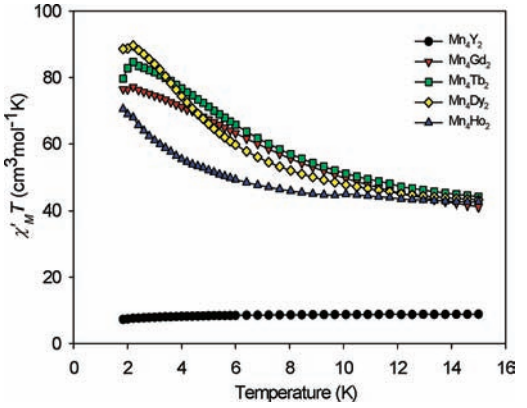

Figure 9. Alternating current susceptibility in-phase (χ'_M) signals at 250 Hz for **1**−**5** in the 1.8−15 K range plotted as $\chi'_M T$ vs T. Solid lines are guides to the eye.

conclusions of the dc studies. The combined dc and ac data for **1** and **5** allow us to rationalize the $S = 12$ ground state of the former as comprising paired Mn^{III} spins as a result of the strong J_{bb} interaction and parallel alignment of the Mn^{II} and Gd^{III} spins due to ferromagnetic interactions to give an $S = 5 + 7 = 12$ ground state. Ferromagnetic interactions involving Gd and transition metals, including Gd and Mn, are with precedent.[12p,24,27] The strong J_{bb} also ensures the $S > 12$ excited states are very high in energy and thus cannot be stabilized sufficiently by dc fields up to 7 T to prevent the saturation value of ~24 μ_B for $S = 12$ being obtained in the reduced magnetization plot. In addition, this explanation also rationalizes the absence of significant anisotropy (D value): as a result of the strong AF coupling of the two Mn^{III} atoms, at low temperature the Mn^{III}_2 pair is in the diamagnetic $S = 0$ ground state and does not contribute to the molecular $S = 12$ giant spin or its anisotropy. In effect, the compound behaves as a $Mn^{II}_2Gd^{III}_2$ complex, and a $D \approx 0$ cm^{-1} value for the ground state is thus to be expected.

The $\chi'_M T$ vs T plots for **2**−**4** are overall similar to that for **1** but also exhibit spin−orbit effects. The large $\chi'_M T$ values coupled with the greater anisotropy of these Ln atoms suggested that **2**−**4** might be new SMMs, but only the Tb analog **2** was found to exhibit out-of-phase ac susceptibility (χ''_M) signals above 1.8 K characteristic of slow magnetization relaxation. **2** exhibits a

dx.doi.org/10.1021/ic201683p |*Inorg. Chem.* 2011, 50, 10476–10485

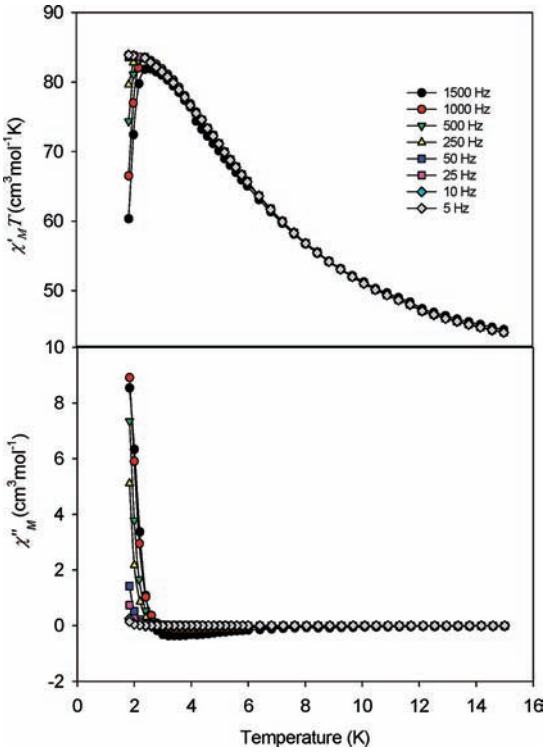

Figure 10. Alternating current susceptibility in-phase χ'_M signal (as $\chi_M'T$) (top) and out-of-phase χ''_M signal (bottom) in the 1.8−15 K range for complex **2** at the indicated frequencies.

frequency-dependent decrease in χ'_MT below ~3 K and a concomitant frequency-dependent χ''_M that is the tail of a peak lying below 1.8 K (Figure 10); it is likely that **3** and **4** also show χ''_M signals but below the 1.8 K limit of our magnetometer. Such χ''_M signals indicate the slow relaxation of magnetization of a SMM, and confirmation of this was sought from hysteresis loop studies.

Single-Crystal Hysteresis Studies for 2 below 1.8 K. Magnetization vs dc field scans for a single crystal of **2**·MeCN at various temperatures and scan rates are shown in Figure 11. Hysteresis loops are evident below a blocking temperature (T_B) of 0.9 K whose coercivity increases with decreasing temperature and increasing scan rate, as expected for SMMs. **2**·MeCN is thus confirmed as a new member of the SMM family. Unusually for a mixed 3d−4f SMM, the hysteresis loops display well-resolved steps due to quantum tunneling of magnetization (QTM) at periodic field values.[28] This was first observed in 3d−4f SMMs for a $Mn_{12}Gd$ complex, where it was assigned to a (relatively) well-isolated ground state, which is not the usual situation when Ln atoms are present.[12l] This was evident as a plateau in χ'_MT below ~5 K, showing ~100% population of the ground state. Complex **2** also displays a plateau in χ'_MT but only at ~2 K, so its ground state is not as well isolated as that of $Mn_{12}Gd$ but still enough to show QTM steps. The hysteresis loop for **2** exhibits a large first step at zero field, where the double-well potential energy curve is symmetric and M_s levels on one side of the barrier are in resonance with those on the other, allowing tunneling to occur through the barrier. Additional steps are also observed at periodic fields when M_s levels are once again brought into resonance. In $Mn_{12}Gd$, the Mn−Gd exchange coupling was enhanced by the many O^{2-} bridges coupling the Gd to the Mn_{12}

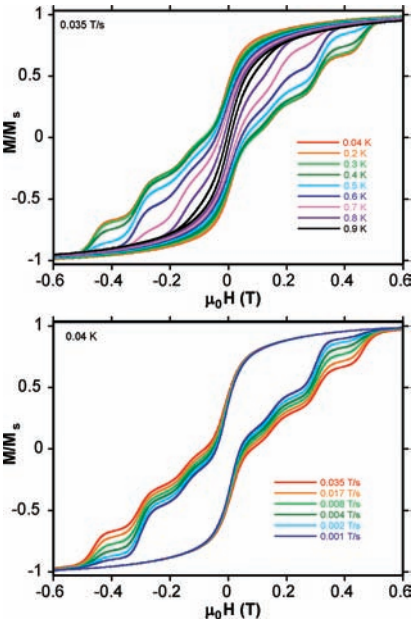

Figure 11. Magnetization (M) vs dc field hysteresis loops for a single crystal of **2**·MeCN at the indicated temperatures with a 0.035 T/s scan rate (top), and the indicated scan rates at 0.04 K (bottom). Magnetization is normalized to its saturation value, M_S.

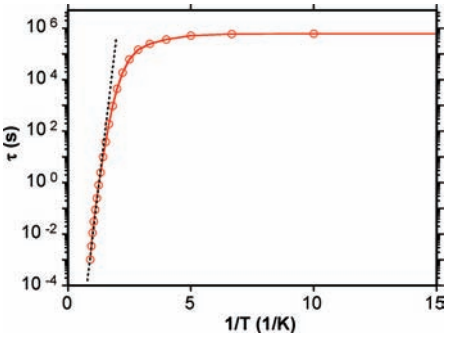

Figure 12. Relaxation time (τ) vs $1/T$ plot for **2**·MeCN constructed using dc magnetization decay data. The dashed line is the fit of the thermally activated region to the Arrhenius equation. See text for fit parameters.

framework. In **2**, there are only two O^{2-} bridges plus four RO^- bridges, so the coupling is expected to be weaker, as the hysteresis loops indicate.

In order to determine the effective barrier (U_{eff}) to magnetization relaxation, relaxation rate vs T data at various temperatures down to 0.04 K were obtained from a magnetization decay vs time study (Figure S3, Supporting Information). The resulting relaxation rate ($1/\tau$) vs T data were used to construct an Arrhenius plot, shown as τ versus $1/T$ in Figure 12, based on the Arrhenius relationship of eq 5

$$\ln(\tau) = \ln(\tau_0) + U_{eff}/kT \quad (5)$$

the characteristic behavior of a thermally activated Orbach process where U_{eff} is the effective energy barrier and k is the Boltzmann constant. The fit to the thermally activated region gave U_{eff} = 20.3 K and $\tau_0 = 1.4 \times 10^{-11}$ s. Below ~0.3 K, the

dx.doi.org/10.1021/ic201683p |*Inorg. Chem.* 2011, 50, 10476–10485

relaxation becomes independent of temperature, consistent with relaxation only via QTM through the anisotropy barrier.

CONCLUSIONS

The initial use of edteH$_4$ in Mn−Ln chemistry has led to four Mn_4Ln_2 (Ln = Gd, Tb, Dy, Ho) complexes, and the corresponding Mn_4Y_2 product was also accessible. The complexes contain a faced-fused double-cubane core that is unprecedented in 3d−4f chemistry, although there are a few examples in homometallic Mn_6 chemistry. This work continues to support edteH$_4$ as a useful route to a variety of new structural types not accessible with other chelates. Detailed magnetic characterization has allowed the nature of the coupling within the core to be characterized, and the Mn_4Gd_2 complex has a large ground state of $S = 12$. When the more anisotropic Ln^{III} atoms are introduced, the Tb^{III} complex **2** was confirmed as a new SMM with an anisotropy barrier (U_{eff}) of 20.3 K. Its blocking temperature is only 0.9 K, but the compound is noteworthy in exhibiting well-resolved QTM steps in the hysteresis loops, characteristic of fairly strong exchange interactions between the Ln and the Mn atoms. Further work with edteH$_4$ is continuing.

ASSOCIATED CONTENT

Supporting Information. X-ray crystallographic files in CIF format for **1**·3MeCN and **2**·MeCN. This material is available free of charge via the Internet at http://pubs.acs.org.

AUTHOR INFORMATION

Corresponding Author

*Phone: +1-352-392-8314. Fax: +1-352-392-8757. E-mail: christou@chem.ufl.edu.

ACKNOWLEDGMENT

We thank the National Science Foundation (CHE-0910472) and the ERC Advanced Grant MolNanoSpin No. 226558 for support of this work.

REFERENCES

(1) (a) Ferreira, K. N.; Iverson, T. M.; Maghlaoui, K.; Barber, J.; Iwata, S. *Science* **2004**, *303*, 1831. (b) Yano, J.; Kern, J.; Sauer, K.; Latimer, M. J.; Pushkar, Y.; Biesiadka, J.; Loll, B.; Saenger, W.; Messinger, J.; Zouni, A.; Yachandra, V. K. *Science* **2006**, *314*, 821.

(2) (a) Ako, A. M.; Hewitt, I. J.; Mereacre, V.; Clérac, R.; Wernsdorfer, W.; Anson, C. E.; Powell, A. K. *Angew. Chem., Int. Ed.* **2006**, *45*, 4926. (b) Moushi, E. E.; Stamatatos, Th. C.; Wernsdorfer, W.; Nastopoulos, V.; Christou, G.; Tasiopoulos, A. J. *Inorg. Chem.* **2009**, *48*, 5049. (c) Stamatatos, Th. C.; Abboud, K. A.; Wernsdorfer, W.; Christou, G. *Angew. Chem., Int. Ed.* **2007**, *46*, 884.

(3) Karotsis, G.; Kennedy, S.; Teat, S. J.; Beavers, C. M.; Fowler, D. A.; Morales, J. J.; Evangelisti, M.; Dalgarno, S. J.; Brechin, E. K. *J. Am. Chem. Soc.* **2010**, *132*, 12983.

(4) Christou, G.; Gatteschi, D.; Hendrickson, D. N.; Sessoli, R. *MRS Bull.* **2000**, *25*, 66.

(5) (a) Sessoli, R.; Gatteschi, D.; Caneschi, A.; Novak, M. A. *Nature* **1993**, *365*, 141. (b) Sessoli, R.; Tsai, H. L.; Schake, A. R.; Wang, S. Y.; Vincent, J. B.; Folting, K.; Gatteschi, D.; Christou, G.; Hendrickson, D. N. *J. Am. Chem. Soc.* **1993**, *115*, 1804.

(6) (a) Bagai, R.; Christou, G. *Chem. Soc. Rev.* **2009**, *38* (4), 1011 and references cited therein. (b) Aromi, G.; Brechin, E. K. *Struct. Bonding (Berlin)* **2006**, *122*, 1. (c) Gatteschi, D.; Sessoli, R. *Angew. Chem., Int. Ed.* **2003**, *42*, 268. (d) Bircher, R.; Chaboussant, G.; Dobe, C.; Gudel, H. U.; Ochsenbein, S. T.; Sieber, A.; Waldmann, O. *Adv. Funct. Mater.* **2006**, *16*, 209. (e) Bogani, L.; Wernsdorfer, W. *Nat. Mat.* **2008**, *7*, 179.

(7) (a) Wernsdorfer, W.; Aliaga-Alcalde, N.; Hendrickson, D. N.; Christou., G. *Nature* **2002**, *416*, 406. (b) Friedman, J. R.; Sarachik, M. P.; Tejada, J.; Ziolo, R. *Phys. Rev. Lett.* **1996**, *76*, 3830. (c) Thomas, L.; Lionti, F.; Ballou, R.; Gatteschi, D.; Sessoli, R.; Barbara, B. *Nature* **1996**, *383*, 145.

(8) Wernsdorfer, W.; Sessoli, R. *Science* **1999**, *284*, 133.

(9) (a) Knill, E. *Nature* **2010**, *463*, 441. (b) Stamp, P. C. E.; Gaita-Ariño, A. *J. Mater. Chem.* **2009**, *19*, 1718. (c) Winpenny, R. E. P. *Angew. Chem., Int. Ed.* **2008**, *47*, 7992. (d) Hill, S.; Edwards, R. S.; Aliaga-Alcalde, N.; Christou, G. *Science* **2003**, *302*, 1015. (e) Meier, F.; Levy, J.; Loss, D. *Phys. Rev. B* **2003**, *68*, 134417. (f) Leuenberger, M. N.; Loss, D. *Nature* **2001**, *410*, 789. (g) Urdampilleta, M.; Cleuziou, J.-P.; Klyastskaya, S.; Ruben, M.; Wernsdorfer, W. *Nat. Mater.* **2011**, *10*, 502.

(10) Osa, S.; Kido, T.; Matsumoto, N.; Re, N.; Pochaba, A.; Mrozinski, J. *J. Am. Chem. Soc.* **2004**, *126*, 420.

(11) Zaleski, C. M.; Depperman, E. C.; Kampf, J. W.; Kirk, M.-L.; Pecoraro, V. L. *Angew. Chem., Int. Ed.* **2004**, *43*, 3912.

(12) (a) Mishra, A.; Wernsdorfer, W.; Parsons, S.; Christou, G.; Brechin, E. K. *Chem. Commun.* **2005**, 2086. (b) Mereacre, V.; Lan, Y.; Clerac, R.; Ako, A. M.; Hewitt, I. J.; Wernsdorfer, W.; Buth, G.; Anson, C. E.; Powell, A. K. *Inorg. Chem.* **2010**, *49*, 5293. (c) Akhtar, M. N.; Zheng, Y.-Z.; Lan, Y.; Mereacre, V.; Anson, C. E.; Powell, A. K. *Inorg. Chem.* **2009**, *48*, 3502. (d) Mereacre, V.; Akhtar, M. N.; Lan, Y.; Ako, A. M.; Clerac, R.; Anson, C. E.; Powell, A. K. *Dalton Trans.* **2010**, *39*, 4918. (e) Liu, C.-M.; Zhang, D.-Q.; Zhu, D.-B. *Dalton Trans.* **2010**, *39*, 11325. (f) Mereacre, V.; Ako, A. M.; Clérac, R.; Wernsdorfer, W.; Hewitt, I. J.; Anson, C. E.; Powell, A. K. *Chem.—Eur. J.* **2008**, *14*, 3577. (g) Zaleski, C. M.; Depperman, E. C.; Kampf, J. W.; Kirk, M. L.; Pecoraro, V. L. *Angew. Chem., Int. Ed.* **2004**, *43*, 3912. (h) Langley, S. K.; Moubaraki, B.; Murray, K. S. *Dalton Trans.* **2010**, *39*, 5066. (i) Mereacre, V.; Prodius, D.; Ako, A. M.; Kaur, N.; Lipkowski, J.; Simmons, C.; Dalal, N.; Geru, I.; Anson, C. E.; Powell, A. K.; Turta, C. *Polyhedron* **2008**, *27*, 2459. (j) Mishra, A.; Wernsdorfer, W.; Abboud, K. A.; Christou, G. *J. Am. Chem. Soc.* **2004**, *126*, 15648. (k) Mereacre, V. M.; Ako, A. M.; Clérac, R.; Wernsdorfer, W.; Filoti, G.; Bartolomé, J.; Anson, C. E.; Powell, A. K. *J. Am. Chem. Soc.* **2007**, *129*, 9248. (l) Stamatatos, T. C.; Teat, S. J.; Wernsdorfer, W.; Christou, G. *Angew. Chem., Int. Ed.* **2009**, *48*, 521. (m) Ako, A. M.; Mereacre, V.; Clerac, R.; Wernsdorfer, W.; Hewitt, I. H.; Anson, C. E.; Powell, A. K. *Chem. Commun.* **2009**, 544. (n) Majeed, Z.; Mondal, K. C.; Kostakis, G. E.; Lan, Y.; Anson, C. E.; Powell, A. K. *Dalton Trans.* **2010**, *39*, 4740. (o) Papatriantafyllopoulou, C.; Wernsdorfer, W.; Abboud, K. A.; Christou, G. *Inorg. Chem.* **2011**, *50*, 421. (p) Rigaux, G.; Inglis, R.; Morrison, S.; Prescimone, A.; Cadiou, C.; Evangelisti, M.; Brechin, E. K. *Dalton Trans.* **2011**, *40*, 4797.

(13) (a) Bagai, R.; Abboud, K. A.; Christou, G. *Inorg. Chem.* **2008**, *47*, 621.(b) Saha, A.; Abboud, K. A.; Christou, G. Manuscript in preparation. (c) Saha, A.; Gangopadhyay, S.; Nehrkorn, J.; Milazzo, R.; Masunov, A. E.; Waldmann, O.; Mutka, H.; Abboud, K. A.; Wernsdorfer, W.; Christou, G. Manuscript in preparation. (e) Bagai, R.; Daniels, M. R.; Abboud, K. A.; Hill, S.; Christou, G. *Inorg. Chem.* **2008**, *;47*, 3318.

(14) Yu, S. B.; Shweky, I.; Lippard, S. J.; Bino, A. *Inorg. Chem.* **1992**, *31*, 3502.

(15) Vandersluis, P. S., A. L. *Acta Crystallogr.; Sect. A* **1990**, *46*, 194.

(16) Davidson, E. R. *MAGNET*; Indiana University: Bloomington, IN, 1999.

(17) Wernsdorfer, W. *Adv. Chem. Phys.* **2001**, *118*, 99.

(18) Wernsdorfer, W.; Chakov, N. E.; Christou, G. *Phys. Rev. B* **2004**, *70* (132413), 1–4.

(19) (a) Liu, W. T.; Thorp, H. H. *Inorg. Chem.* **1993**, *32*, 4102. (b) Palenik, G. *J. Inorg. Chem.* **1997**, *36*, 4888. (c) Brown, I. D.; Wu, K. K. *Acta Crystallogr., Sect. B: Struct. Sci.* **1976**, *32*, 1957.

(20) (a) Godbole, M. D.; Roubeau, O.; Mills, A. M.; Kooijman, H.; Spek, A. L.; Bouwman, E. *Inorg. Chem.* **2006**, *45*, 6713. (b) Taguchi, T.; Daniels, M. R.; Abboud, K. A.; Christou, G. *Inorg. Chem.* **2009**, *48*, 9325.

(c) Igashira-Kamiyama, A.; Kajiwara, T.; Nakano, M.; Konno, T.; Ito, T. *Inorg. Chem.* **2009**, *48*, 11388. (d) Langley, S. K.; Chilton, N. F.; Massi, M.; Moubaraki, B.; Berry, K. J.; Murray, K. S. *Dalton Trans.* **2010**, *39*, 7236.

(21) Ritchie, C.; Ferguson, A.; Nojiri, H.; Miras, H. N.; Song, Y.-F.; Long, D.-L.; Burkholder, E.; Murrie, M.; Kogerler, P.; Brechin, E. K.; Cronin, L. *Angew. Chem., Int. Ed.* **2008**, *47*, 5609.

(22) Yang, E.-C.; Harden, N.; Wernsdorfer, W.; Zakharov, L.; Brechin, E. K.; Rheingold, A. L.; Christou, G.; Hendrickson, D. N. *Polyhedron* **2003**, *22*, 1857.

(23) Kambe, K. *J. Phys. Soc. Jpn.* **1950**, *5*, 48.

(24) (a) Canada-Vilalta, C.; Huffman, J. C.; Christou, G. *Polyhedron* **2001**, *20*, 1785. (b) Aromí, G.; Bhaduri, S.; Artús, P.; Huffman, J. C.; Hendrickson, D. N.; Christou, G. *Polyhedron* **2002**, *21*, 1779–1786.

(25) Roubeau, O.; Clérac, R. *Eur. J. Inorg. Chem.* **2008**, 4325 and references therein.

(26) Benelli, C.; Murrie, M.; Parsons, S.; Winpenny, R. E. P. *J. Chem. Soc., Dalton Trans.* **1999**, 4125.

(27) Benelli, C.; Gatteschi, D. *Chem. Rev.* **2002**, *102*, 2369.

(28) Some representative examples: (a) Chakov, N. E.; Soler, M.; Wernsdorfer, W.; Abboud, K. A.; Christou, G. *Inorg. Chem.* **2005**, *44*, 5304. (b) Rajaraman, G.; Murugesu, M.; Sanudo, E. C.; Soler, M.; Wernsdorfer, W.; Helliwell, M.; Muryn, C.; Raftery, J.; Teat, S. J.; Christou, G.; Brechin, E. K. *J. Am. Chem. Soc.* **2004**, *126*, 15445. (c) Gatteschi, D.; Sessoli, R. *Angew. Chem., Int. Ed.* **2003**, *42*, 268. (d) Leuenberger, M. N.; Mucciolo, E. M. *Phys. Rev. Lett.* **2006**, *97*, 126601. (e) Wernsdorfer, W.; Caneschi, A.; Sessoli, R.; Gatteschi, D.; Cornia, A.; Villar, V.; Paulsen, C. *Phys. Rev. Lett.* **2000**, *84*, 2965. (f) Yang, E.-C.; Wernsdorfer, W.; Hill, S.; Edwards, R. S.; Nakano, M.; Maccagnano, S.; Zakharov, L. N.; Rheingold, A. L.; Christou, G.; Hendrickson, D. N. *Polyhedron* **2003**, *22*, 1727.